NAVIER-STOKES CFD ASSESSMENT OF TWO MULTI-NOZZLE ANNULAR JET PUMPS WITH A DESIGN OPTIMISATION STUDY

Morrall A.*, Campobasso M.S. and Quayle S.
*Author for correspondence
Department of Engineering,
Lancaster University,
Lancaster, LA1 4YW,
United Kingdom,
E-mail: a.morrall1@lancaster.ac.uk

ABSTRACT

This paper studies a gas-gas multi nozzle annular jet pump, a variant of the annular jet pump configuration. The multi-nozzle jet pump injects the motive fluid through discrete nozzles distributed around the pump bore. Due to their orientation the jets induce swirl downstream of the injection nozzles. A swirling flow is reported in several studies to improve the efficiency of annular jet pumps by improving the mixing between fluids. Two pump designs with differing nozzles orientations are investigated using the commercial CFD code ANSYS® FLUENT with results compared to experimental data. The study explores the sensitivity of grid-independent solutions to selected RANs turbulence models. A design of experiments based on the nozzle orientation of the pumps is then undertaken to assess the effect on performance.

INTRODUCTION

A jet pump is a fluidic device that has no internal moving parts, and transfers the momentum of high-velocity motive jet flow through one or more nozzles to a pipe bore containing a secondary fluid. A multi-nozzle annular jet pump, the subject of this study, discharges the motive fluid into the pipe bore through a number of circumferentially distributed discrete nozzles. The nozzles are angled axially and circumferentially to provide downstream momentum and produce vorticity. For this study, single-phase analysis is used with compressed air considered as the motive fluid and atmospheric air as the secondary fluid.

Numerical simulations are undertaken on two prototype multi-nozzle annular jet pumps (AJPs), shown in Figure 1, analysing flow patterns and turbulence model sensitivity. Simulations are verified against experimental results comparing static wall pressure and axial velocity on the duct centreline. A design of experiments-based optimisation study is then produced, which aims to determine the optimal axial and circumferential inclination of the jets.

NOMENCLATURE

p	[Pa]	Total pressure
Q	[m^3/s]	Volume flow rate
η	[W/m^3]	Efficiency
Special characters		
α	[˚]	Nozzle axial angle
β	[˚]	Nozzle circumferential angle
Subscripts		
m		Motive fluid (compressed air)
s		Secondary fluid (suction)
d		Discharged fluid (combined)

Swirling flow in jet pumps has been shown to improve mixing and entrainment [1] [2], and can be used to increase a jet pumps efficiency. The efficiency of a jet pump, given by Eq 1, is described as the ratio of power gained by the suction fluid, P_{out} to energy provided from the motive fluid, P_{in} [3]. The parameters indicated in Eq. 1 are as follows $Q_m$and Q_s are the volume flow rate for the motive and secondary fluids respectively. p_m, p_s and p_d, represent the total pressure of the motive, secondary and the combined fluid at pumps exit.

$$\eta = \frac{Q_s(p_d - p_s)}{Q_p(p_p - p_d)} \quad (1)$$

The optimal level of swirl of a single 360º nozzle AJP has been a subject for a number of studies. In an experimental study of water based AJPs by Shimizu [12] guide vanes are used on the motive fluid to induce swirl. The results compared the performance of an AJP with no inlet swirl, against varying intensities of inlet swirl and found high levels of swirl to be detrimental, reducing performance due to increased frictional and mixing losses. A small level of swirl improved efficiency compared to no swirl. In a separate experimental study on a water based AJP, a moderate level of induced swirl was also shown to increase pump efficiency [4].

The circumferential inclination of the nozzles can be modified to induce the optimal level of swirl. The multi-nozzle AJP though is an uncommon design with little research devoted to the design of pump. The axial angle of a multi-nozzle jet pump, ranging from 11° to 19°, was experimentally tested to measure the effect on induced water mass flow rate [5]. It was found that the 19° angle produced the highest mass flow rate, though efficiency did not correlate with an increasing/decreasing axial angle. Thus, it was concluded that the jets axial momentum

was not the dominant effect on pump efficiency. Another experimental assessment of an airlift pump, similar in design to a multi-nozzle AJP, was set up to test the effect of swirl and found that high levels of swirl reduced the flow rate of the pump [6].

This paper starts by detailing the pump and apparatus used for the analyses. In the following sections the software and methods for numerical simulations are discussed. The results from the experimental and turbulence model assessment of the two prototype pumps are then presented. The results of the design of experiments optimisation study are given, and the presented study is summarised in the final section.

MULTI-NOZZLE ANNULAR JET PUMP

One of the pumps tested is shown in Figure 1, with the general internal structure schematic shown in Figure 2. The pump is comprised of four parts: the motive inlet, the annulus, the nozzles and the pump bore. The axial and circumferential angles of the nozzles are given by α and β respectfully. For the two considered AJPs the geometry of motive inlet, annulus, nozzle diameter and pump bore are held constant, and only the angle α of the nozzles is changed. For Pump 1, a low axial angle, α, is used, whilst for Pump 2 a high angle of α is considered. For both pumps the same, value of β is used which adds a considerable degree of swirl at injection.

In an earlier work, which this paper supersedes with a more realistic numerical setup and use of different grids, the injection of the motive fluid in Pumps 1 and 2 is analysed [7]. It was found that Pump 2 imparted a significant radial velocity, with the discrete jets forming an annular flow pattern downstream of injection. Pump 1 also resulted in annular flow regime with a larger axial component of flow.

TEST RIG

The test rig schematic is shown in Figure 3. It consists of a multi-nozzle AJP connected to a ½ Inch British standard pipe compressed airline and two unequal length pipes, Pipe X (Suction side) and Pipe Y (Discharge side). The dimensions of the pump and experimental rig are given in Table 1. To modify and measure the compressed air flow into the pump, a throttle valve, a pressure gauge and volume flow meter are connected upstream on the compressed air line. The motive pressure is adjusted using the throttle valve in the rig and measured using an analogue Bourdon tube pressure gauge. The compressed air pressure for this analysis is set at 2 bar.

Pipe X has 12 flush mounted linearly inserted pressure taps, whilst Pipe Y has 19 pressure taps circumferentially and linearly distributed; so mean values of pressure at differing circumferential positions downstream of the pump can be measured. Readings are taken using a Kane 3200 Differential Pressure Meter, which has a range of +/- 9999 Pa to a resolution of 1 Pa. A Pitot tube is also placed along the central axis to measure axial velocity. Digital readings are cross-referenced with a fluid column multi-manometer to ensure accurate calibration.

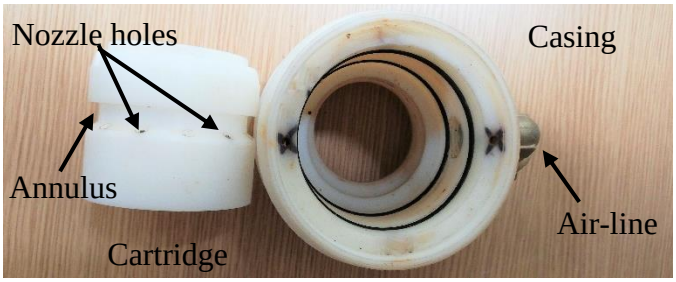

Figure 1: *Prototype Multi-Nozzle Annular Jet Pump*

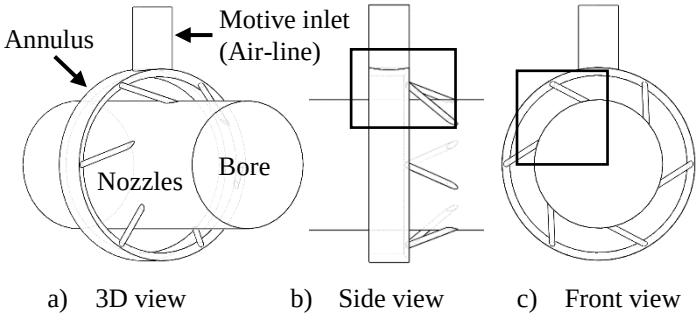

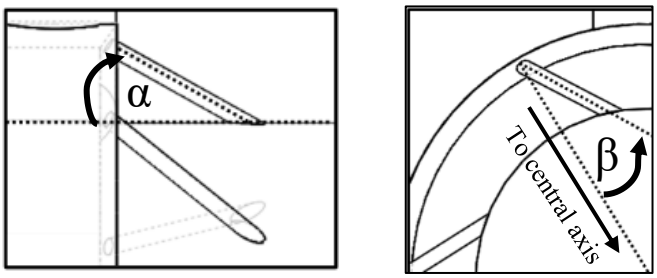

Figure 2*: Schematic layout multi-nozzle annular jet pump*

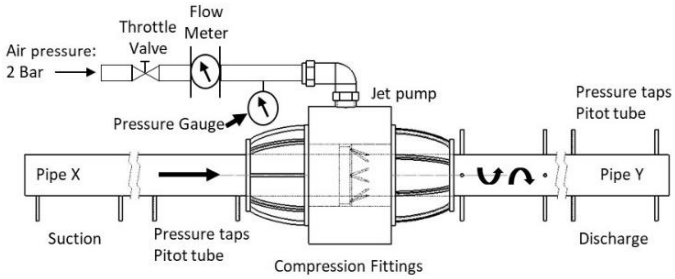

Figure 3*: Test rig schematic*

Table 1. Experimental Rig & Pump Dimensions

Pump Geometry	Dimension
Pipe Bore Diameter	*50 mm*
Motive Inlet Pipe Diameter	*12.7 mm*
Number of Nozzles	*6*
Nozzle Diameter	*2 mm*
Pipe X: Inlet Pipe Length	*600 mm*
Pipe Y: Outlet Pipe Length	*700 mm*
Pump length	*130 mm*
Axial angle [α]	*Pump 1:35°* *Pump 2: 65°*
Radial angle [β]	*20°*

NUMERICAL SETUP

CFD Code

CFD simulations use the commercial finite volume code, ANSYS® FLUENT, Release 19.1. A compressible flow model with the pressure-based COUPLED solver is used for numerical integration with the spatial discretisation of the governing equations being second order accurate.

Computational grid

The physical domain and an illustration of the mesh are shown in Figure 4. The mesh is produced using ANSYS Meshing, and consists of several sub-domains, enabling a mix of hexahedral and tetrahedral meshes. The boundary layers are simulated by ensuring an adequate cell count through inflation layering along all walls, so the non-dimensionalised wall distance, y+ of the first nodes off the walls from the walls themselves is of order 1. Four levels of mesh refinement are considered with parameters defined in Table 2. Boundary conditions are indicated in Fig. 4. Total pressure is prescribed at both inlet boundaries; 0 Pa for the secondary inlet , so the mass flow induced can vary and 200000 Pa for the motive inlet. The pressure outlet has the radial equilibrium condition applied, with the axial pressure prescribed from experimental measurements.

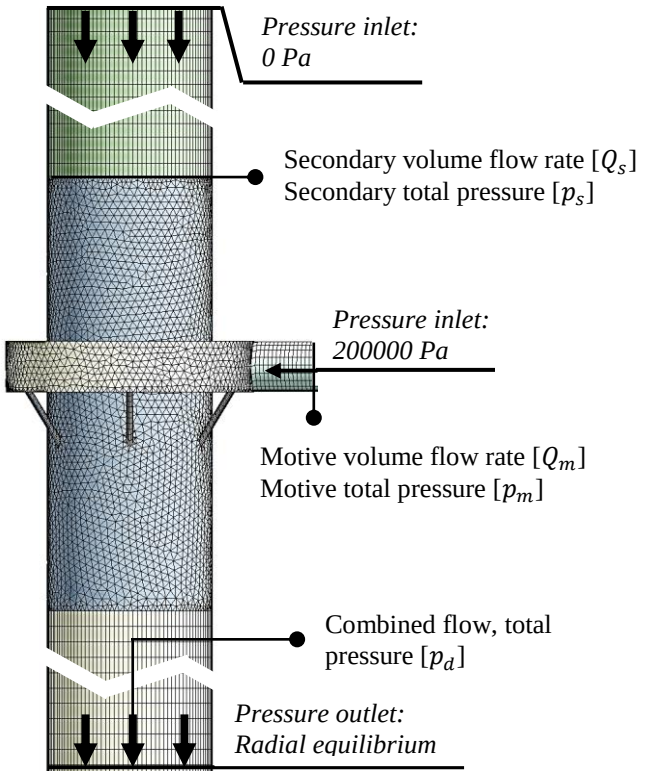

***Figure 4**: Computational grid and boundary conditions.*

Table 2. Spatial grid refinement

Mesh level	Cell Count [*million*]	Naming convention
1	6.25	Coarse
2	12.5	Medium
3	25.0	Fine
4	50.0	Extra fine

Turbulence models

The RANs turbulence models considered in this study are the k-ω Shear stress transport (SST) eddy viscosity model, and the Reynolds stress model (RSM). The k-ω SST model, is a two-equation model based on Boussinesq approximation [8]. The model combines the k-ε and k-ω models through blending functions; utilising the k-ε model in the far-field and the k-ω model near the wall. This approach benefits from the advantages of both models, so that the boundary layer is modelled without the need for wall functions and the solution is insensitive to the selected free stream level of the specific dissipation rate. The equations for the compressible k-ω SST can be found in [9].

The RSM is a higher order RANS model that solves a transport equation for each of the components of the Reynolds stress tensor [9]. To close the transport equations an additional term for the dissipation rate is also modelled . The method does not rely on Boussinesq's approximation, as the Reynolds stresses are solved and not related directly and linearly to the mean flow strain tensor. Thus, the RSM approach accounts for the important effect of the transport of the principal turbulent shear-stress. The equations for the compressible RSM model can found in [9].

RESULTS

The simulation results for both pumps are compared against experimental data, with spatial grid convergence assessed using up to four levels of refinement. A few numerical instabilities were found with the extra fine mesh, so some of these are not assessed. It is found that steady state analysis provided suitable convergence and accuracy with unsteady simulations adding little acumen to the assessment. Results presented in graphical form show the flow from left to the right through the pipe, with labels indicating the suction and outlet pipes accordingly. The injection point is also marked on the graphs to specify where the motive fluid is injected into the bore. Figures compare computed values of static wall pressure and axial velocity against the experimental results.

The results of the k-ω SST and RSM simulations for Pump 1 are presented in Figures 5-6 respectfully. Both the k-ω SST model and the RSM show suitable accuracy in comparison to the experimental data. From these figures grid independence for the k-ω SST is difficult to ascertain. A close analysis however shows that after injection the computed axial velocity of medium grid varies when compared to the other mesh levels. This is attributed to the capturing of the expanding jets of motive air and their influence on the core of the flow. The results of the RSM also show differences in velocity after injection, though the static wall pressure values for the other meshes compare well.

The performance parameters for Pump 1, referring to Equation (1) and Figure 4, are presented in Table 3-4. These results highlight that spatial convergence for the kω-SST model is achieved using the fine mesh. Unfortunately, due to numerical stability issues, the extra fine solution is not available for the RSM, however it is noted that a similar trend exists between the two turbulence models, and as such it is expected that the fine grid is a grid independent solution. The pressure and velocity curves and the efficiency predicted for Pump 1 by the two models is also comparable.

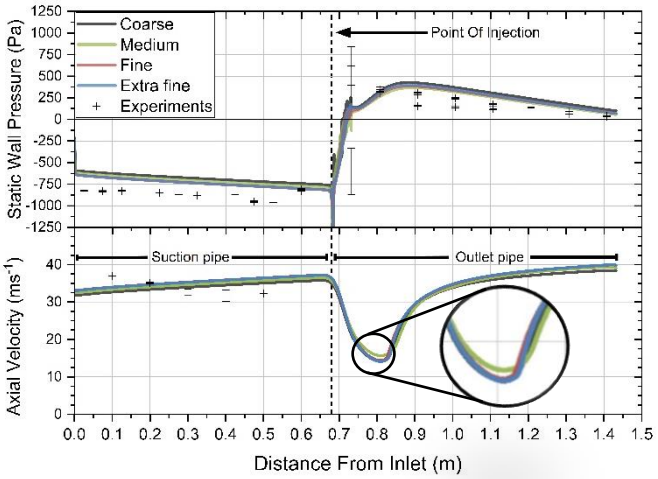

***Figure 5**: Pump 1 kω-SST Grid refinement and experiments*

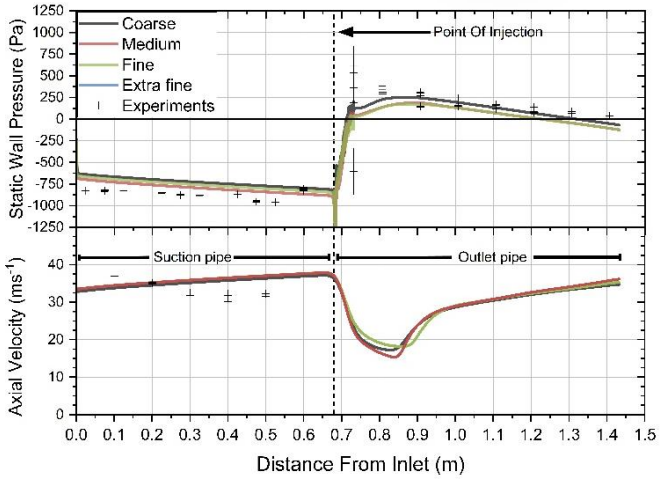

***Figure 6**: Pump 1 RSM Grid refinement and experiments*

Table 3. Pump 1, kω SST performance metrics

Parameter	***Coarse***	***Medium***	***Fine***	***Extra fine***
$Q_s \times 10^{-3}$ [m^3/s]	62.0	63.3	64.6	64.5
$Q_m \times 10^{-3}$ [m^3/s]	2.97	2.97	2.99	2.98
$p_d \times 10^2$ [Pa]	8.96	8.84	9.26	9.23
$p_s \times 10^2$ [Pa]	-1.31	-1.35	-1.39	-1.39
$p_m \times 10^5$[Pa]	2.00	2.00	2.00	2.00
Efficiency [%]	10.78	10.89	11.57	11.52

Table 4. Pump 1, RSM, performance metrics

Parameter	***Coarse***	***Medium***	***Fine***	***Extra fine***
$Q_s \times 10^{-3}$ [m^3/s]	64.1	65.4	67.0	-
$Q_m \times 10^{-3}$ [m^3/s]	2.94	2.94	2.94	-
$p_d \times 10^2$ [Pa]	7.68	7.46	7.79	-
$p_s \times 10^2$ [Pa]	-1.44	-1.48	-1.56	-
$p_m \times 10^5$[Pa]	2.00	2.00	2.00	-
Efficiency [%]	9.99	9.97	10.69	-

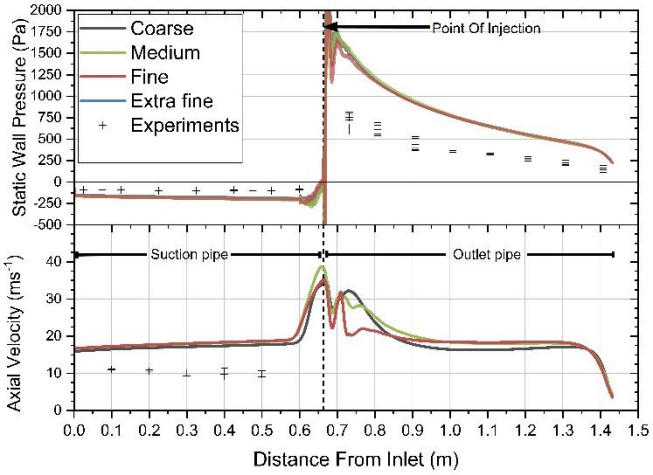

***Figure 7**: Pump 2 kω-SST Grid refinement and experiments*

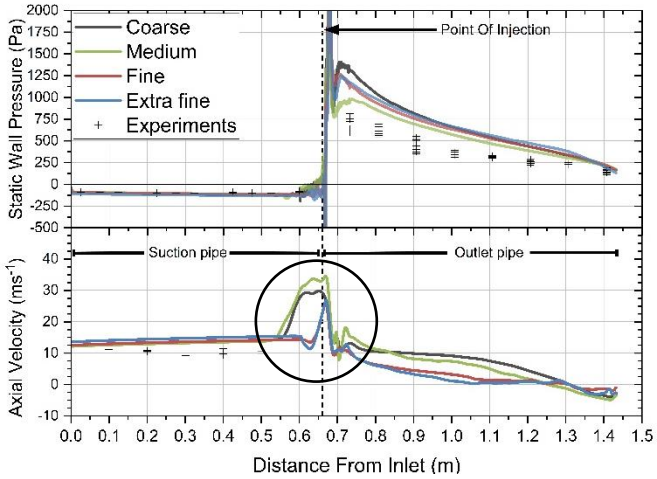

***Figure 8**: Pump 2 RSM Grid refinement and experiments*

Table 5. Pump 2, kω SST, performance metrics

Parameter	***Coarse***	***Medium***	***Fine***	***Extra fine***
$Q_s \times 10^{-3}$ [m^3/s]	42.5	32.5	39.1	-
$Q_m \times 10^{-3}$ [m^3/s]	2.90	2.91	2.92	-
$p_d \times 10^2$ [Pa]	4.52	4.71	4.74	-
$p_s \times 10^2$ [Pa]	8.64	-4.74	-2.27	-
$p_m \times 10^5$[Pa]	2.00	2.00	2.00	-
Efficiency [%]	2.68	2.91	3.33	-

Table 6. Pump 3, RSM, performance metrics

Parameter	***Coarse***	***Medium***	***Fine***	***Extra fine***
$Q_s \times 10^{-3}$ [m^3/s]	58.4	56.4	24.3	26.0
$Q_m \times 10^{-3}$ [m^3/s]	2.89	2.89	2.90	2.89
$p_d \times 10^2$ [Pa]	3.25	3.18	2.85	2.10
$p_s \times 10^2$ [Pa]	1.19	1.33	-0.238	-0.261
$p_m \times 10^5$[Pa]	2.00	2.00	2.00	2.00
Efficiency [%]	2.08	1.81	1.29	1.07

The results for Pump 2 are shown in Figures 7-8 and Tables 5-6. Figure 7 and Table 5 indicate the grid solutions for the kω-SST model and likewise in Figure 8 and Table 6 the results of RSM are presented. The solution of the kω-SST turbulence model greatly over predicts suction and discharge pressures, as well as the axial velocity through the domain. Pump 2, which has a larger α angle than Pump 1 produces higher levels of circumferential flow. This over prediction over pressure and velocity is due to deficiencies of the kω-SST turbulence model with highly swirling flows, where the model has difficulties with the mean flow streamline curvature [10]. The over prediction is further evidenced at the end of the domain where a drop in pressure and axial velocity occurs as the simulation meets the enforced experimentally imposed exit axial pressure. Graphically the RSM model shows significantly better results for both the static wall pressure and axial velocity calculations.

Grid convergence for Pump 2 is difficult to assess, with the kω-SST model showing no observable trend toward convergence at the fine mesh size. The velocity spike before the injection, highlighted in Figure 8, for the coarse and medium meshes also adversely affects the results of the RSM and as such there is significant differences between the results of coarse/medium meshes compared to the fine/extra fine meshes. The predicted performance for Pump 2 is also much lower than that of Pump 1 and is indicative of the chaotic flow downstream of injection, which neither model is shown to accurately capture.

DESIGN OF EXPERIMENT ANALYSES

The design of experiments (D.O.E) tests a range of axial and circumferential angles that fit within the specified limits of the pump casing shown in Figure 1. For the D.O.E, the kω-SST model is selected, despite the model having inferior prediction compared to experiments. This model is chosen on the basis that Pump 2 is significantly worse than Pump 1 and as such there will be focus towards the geometry of Pump 1, where the differences of the two models are not so large. The kω-SST model is also computationally much quicker to run than RSM.

The computational domain and set-up for the D.O.E is shown in Figure 9. The previously enforced boundary condition at the exit to the domain can no longer be applied as this was measured for each pump. The new domain has an additional box at the end of the discharge pipe to represent venting to atmosphere; with the faces of the box are prescribed as a pressure outlet of 0 Pa. The 'fine' mesh settings as used in the previous analyses are applied to build the new mesh. The results of the new mesh are also cross-compared with the previous analyses with the same results achieved in both cases, for Pumps 1 and 2.

The D.O.E uses 35 simulations of varying angles to build a response surface that can be used to indicate the axial and radial nozzle angles that produce the highest efficiency, Equation (1). For this analysis, the bore size, the number of nozzles and size of nozzles is kept constant, so they are similar to Pumps 1 and 2. The D.O.E makes use of ANSYS's built in software, where the nozzle angles are assigned as parametric value within computer aided design software, ANSYS Design Modeller. The ANSYS solver updates the geometry accordingly and reapplies the mesh settings before solving the computational flow field. The performance parameters for each simulation are recorded, and are used to develop the response surface. The response surface is generated with Genetic aggregation algorithm within ANSYS Design exploration [11], and compares the nozzle angles against the efficiency metric.

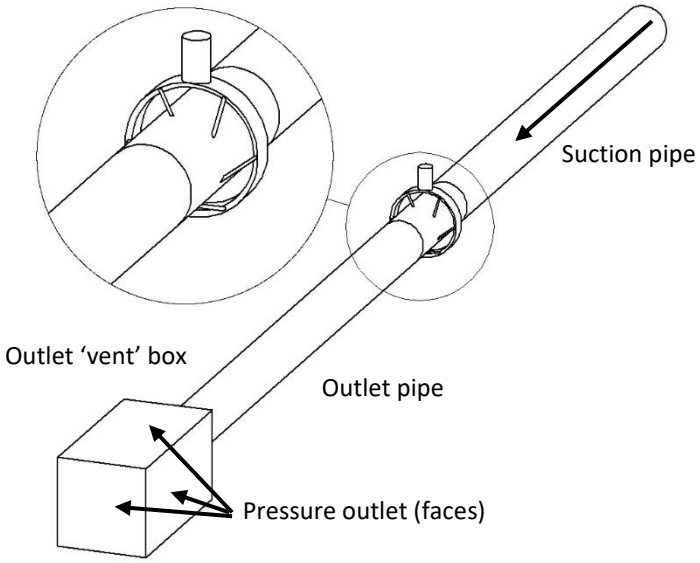

***Figure 9**: Design of experiments computational domain.*

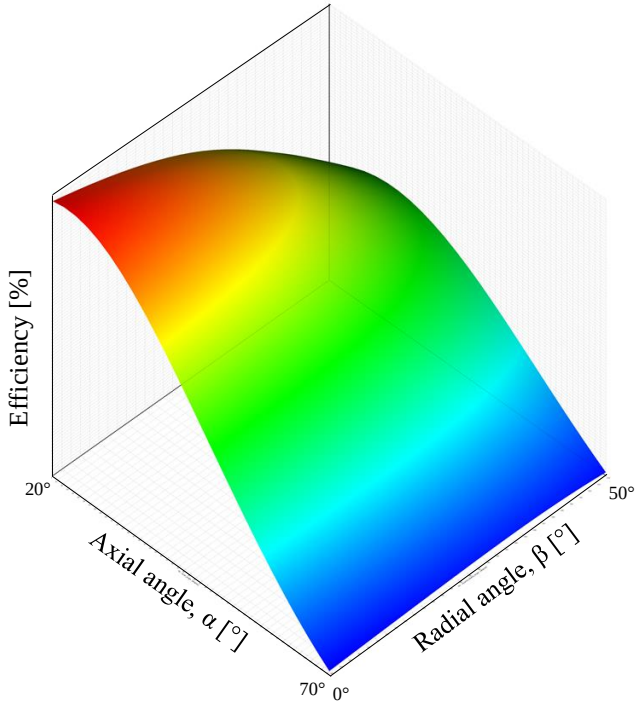

***Figure 10**: Design of experiments response surface*

The results of the D.O.E show that a low axial angle, between 20° and 30°, and a low radial angle produce the highest efficiency. This ratifies the analysis on Pumps 1 (Low α) and Pump 2 (High α). It follows that a low axial angle can transfer more axial momentum to the secondary fluid, hence the higher efficiencies observed. In all cases a large circumferential angle,

which produces a high level of swirl is shown to decrease the pump efficiency. This effect is also observed in the single nozzle AJP [12]. It is expected that there is an optimal efficiency for which the value of β is larger than zero as reported in literature [1] [2], for which the results of this analysis are inconclusive and would require further analysis to increase resolution in this region.

FLOW ANALYSES

To understand the effect of the nozzle angles, the results of kω-SST simulations are used to analyse the internal flow mechanisms. In the comparison shown in Figure 11 a-f, a comparison is made between Pump 1 for which the motive nozzle has a moderate circumferential angle against a pump with no circumferential inclination. The axial angle is constant for both cases and is equal to 35°.

Figures 11- a, c, e, show that that a moderate β angle results in the discrete jets forming an annular flow pattern as the motive fluid swirls around the periphery of the pipe. Where there is no circumferential angle, the motive fluid is shown to interact in the core of the pipe, Figures 11- b, d, f. As there is no wall friction in the middle of the pump this will have a significant effect on the pumps efficiency; as the flow is not wall bounded there is no energy dissipated interacting with the wall. The annular flow pattern also contains two shear layers, so further losses in the efficiency of flow are incurred, compared to that of the central axis oriented flow. The pump with no circumferential component also induces much more mass flow, indicating the central axis flow also entrains more of the secondary fluid.

CONCLUSIONS

A thorough assessment is made on two multi-nozzle AJPs, comparing the numerical accuracy of two RANs models, the kω-SST and the RSM. It was found that the RSM more accurately predicted the fluid flow through both pumps, whereas for a flow with a reduced level swirl the kω-SST model was sufficient. A design of experiments based optimisation was then undertaken to assess the impact of nozzle axial and circumferential angle on the pumps efficiency. It was found that reducing the circumferential inclination of the nozzle improved jet pump performance as this resulted in a central axis orientated flow, whereas increasing the circumferential angle resulted in an annular flow in the pipe, subject to frictional losses and two shear layers.

ACKNOWLEDGEMENTS

This work is supported by the Centre for Global Eco Innovation and the ERDF. Design of the multi-nozzle AJP is credited to TCL Cumbria with which this work is presented in partnership. Special thanks to industry advisor, Ian Stephenson. Simulations are run on the Lancaster High End Computing (HEC) Cluster.

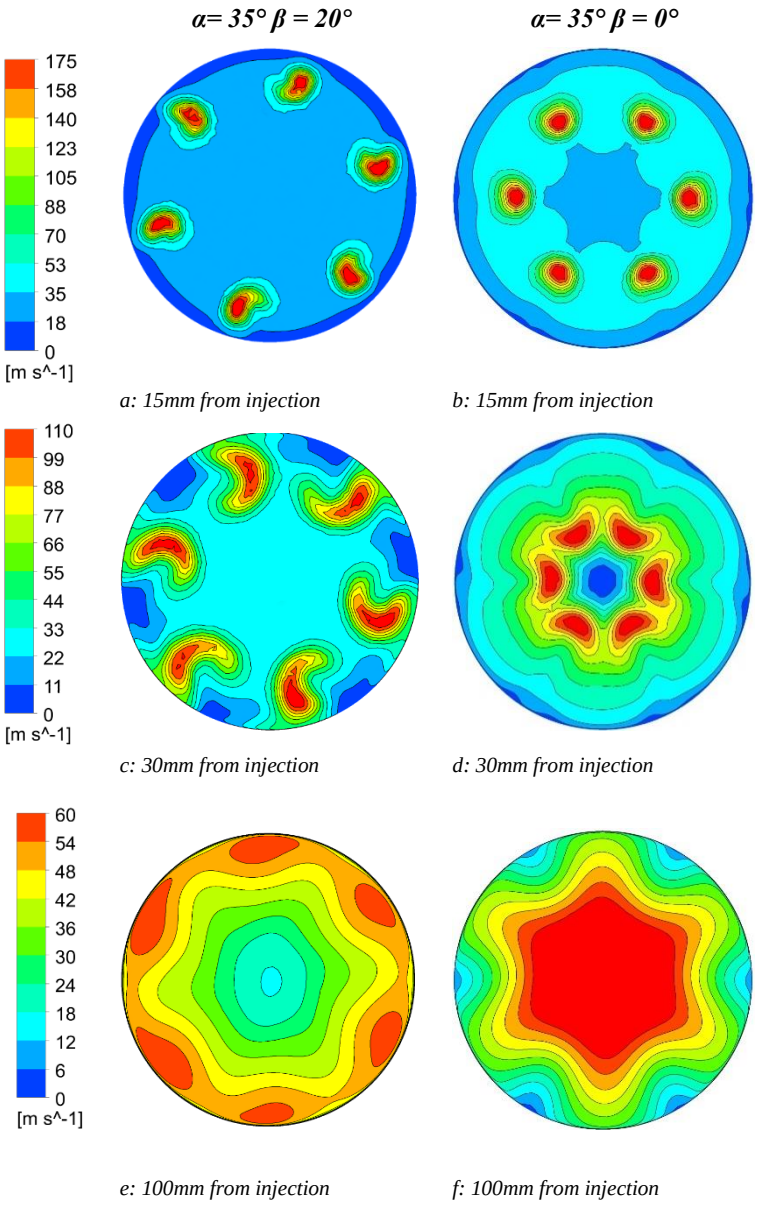

***Figure 11**: Flow velocity comparison of radial nozzle angle*

REFERENCES

[1] H. J. Sheen, W. J. Chen and S. Y. Jeng, "Recirculation zones of unconfined and confined annular swirling jets," *AIAA J,* vol. 34, pp. 572-579, 1996.

[2] G. A. Siamas, X. Jiang and L. C. Wrobel, "Dynamics of Annular Gas–liquid Two-phase Swirling Jets," *International Journal of Multiphase Flow,* vol. 35, no. 5, pp. 450-467, 2009.

[3] S. H. Winoto, H. Li and D. A. Shah, "Efficiency of Jet Pumps," *Journal of Hydraulic Engineering,* p. 126, 2000.

[4] D. W. Guillaume and T. A. Judge, "Improving the efficiency of a jet pump using a swirling primary jet," *Review of Scientific Instruments,* pp. 553-555, 2004.

[5] F. N. Lee, G. A. McDonnel and M. F. Kegel, “The Effects of Jet Angle and Geometry on the Performance of the Jet Assisted Air Lift Pump,” Fisheries & Aquatic Sciences, 1981.

[6] J. Riglin, “Performance Characteristics of Airlift Pumps with Vortex Induced by Tangential FLuid Injection,” Buknell Digital Commons, Bucknell University, 2011.

[7] A. Morrall, M. S. Campobasso and S. Quayle, “Numerical and experimental investigation of a vortical flow-inducing jet pump,” in *Conference on Modelling Fluid Flow*, Budapest, 2018.

[8] F. R. Menter, “Two-Equation Eddy-Viscosity Turbulence Models For Engineering Application,” *AIAA*, vol. 32, no. 8, pp. 1598-1605, 1994.

[9] D. C. Wilcox, Turbulence modeling for CFD, La Cãnada: DCW Industries, 2010.

[10] S. Jakirlic, K. Hanjalic and C. Tropea, “Modeling rotating and swirling turbulent flows: a perpetual challenge,” *AIAA*, vol. 40, no. 10, pp. 1984-1996, 2002.

[11] ANSYS (R) Academic Research FLuent, “Theory Guide,” ANSYS, 2018.

[12] Y. Shimizu, S. Nakamura, S. Kuzuhara and S. Kurata, “Studies of the Configuration and Performance of Annular Type Jet Pumps,” vol. 109, no. 3, 1987.